


Article

# Sampling Confined Fission Tracks for Constraining Geological Thermal Histories

Raymond Jonckheere <sup>1,\*</sup> , Carolin Aslanian <sup>1,†</sup>, Hongyang Fu <sup>1,2,†,‡</sup> and Florian Trilsch <sup>1,†</sup>

<sup>1</sup> Endogene Geologie, TU Bergakademie Freiberg, Bernhard-von-Cotta-Straße 2, D09599 Freiberg, Germany; carolin.aslanian23@gmail.com (C.A.); fuhongyang@cug.edu.cn (H.F.); florian.trilsch@doktorand.tu-freiberg.de (F.T.)

<sup>2</sup> Key Laboratory of Tectonics and Petroleum Resources, China University of Geosciences, Wuhan 430074, China

\* Correspondence: raymond.jonckheere@geo.tu-freiberg.de

† These authors contributed equally to this work.

‡ Present address: Chuanqing Drilling Engineering Ltd., CNPC, Chengdu 610051, China.

**Abstract:** Fission-track modeling rests on etching, counting and measuring the lattice damage trails from uranium fission. The tools for interpreting fission-track data are advanced but the results are never better than the data. Confined-track samples must be an adequate size for statistical analysis, representative of the track population and consistent with the model assumptions and with the calibration data. Geometrical and measurement biases are understood and can be dealt with up to a point. However, the interrelated issues of etching protocol and track selection are more difficult to untangle. Our investigation favors a two-step protocol. The duration of the first step is inversely proportional to the apatite etch rate so that different apatites etch to the same  $Dpar$ . A long immersion reveals many more confined tracks, terminated by basal and prism faces. This allows consistent length measurements and permits orienting each track relative to the  $c$ -axis. Long immersion times combined with deep ion irradiation reveal confined tracks deep inside the grains. Provided it is long enough, the precise immersion time is not important if the effective etch times of the selected tracks are calculated from their measured widths. Then, whether the sample is mono- or multi-compositional, we can, post hoc, select tracks with the desired properties. The second part of the protocol has to do with the fact that fossil tracks in geological samples appear to be under-etched compared to induced tracks etched under the same conditions. This should be assumed if the semi-axes of a fitted ellipse plot above the induced-track line. In that case, an additional etch can increase the track lengths to a point where they are consistent with the model based on lab-annealing of induced tracks, a condition for valid thermal histories. Here too, it is possible to select a subset of tracks with effective etch times consistent with the model if the widths of confined tracks are measured along with their lengths and orientations.

**Keywords:** apatite; fission-track; confined tracks; etching protocols; sampling biases; geothermal histories



**Citation:** Jonckheere, R.; Aslanian, C.; Fu, H.; Trilsch, F. Sampling Confined Fission Tracks for Constraining Geological Thermal Histories. *Minerals* **2024**, *14*, 1016. <https://doi.org/10.3390/min14101016>

Academic Editors: Ruxin Ding, Honghua Lv and Rong Yang

Received: 4 September 2024

Revised: 5 October 2024

Accepted: 6 October 2024

Published: 8 October 2024



**Copyright:** © 2024 by the authors. Licensee MDPI, Basel, Switzerland. This article is an open access article distributed under the terms and conditions of the Creative Commons Attribution (CC BY) license (<https://creativecommons.org/licenses/by/4.0/>).

## 1. Introduction

The fission-track method for dating and retracing the thermal histories of geological samples is based on counting and measuring the damage trails from spontaneous uranium fission in minerals. Apatite is the most important mineral: separated grains are mounted in resin, polished and etched for microscopic inspection. Etching creates channels along the damage trails. Etched fission tracks have distinctive shapes and dimensions depending on their orientation and that of the etched surface. It is not apparent how their numbers and lengths are related to those of the unetched tracks. For that reason, experimental protocols and calibration against age standards must guarantee accurate modeling results.

This contribution deals with matters related to etching, selection and measurement of confined fission tracks. The requirements of a confined-track sample are that it is of a sufficient size for statistical treatment, representative of the track population, consistent with

the modeling assumptions and calibration data, and that the measurements are reproducible and consistent between analysts. Previous studies showed that the variation of the mean track length amounts to ~3% for replicate measurements by an experienced scientist and ~5% for different scientists measuring the same sample [1–4]. It is <0.5% for two scientists measuring the same track images [5]. However, it rises to  $\gtrsim 10\%$  for complex samples [4] and when the results of different etching and measurement protocols are compared [6–8]. Although we know of no statistical comparisons, it is certain that the track length distributions are less reproducible than their means (Figure 7 in [4]; Figure 2 in [9]). Several factors are known to bias confined-track measurements. Following [4], we distinguish between geometrical biases, etching biases, observer biases and measurement biases.

Geometrical biases include length and orientation bias, fracture and host-track thickness bias, edge- and surface-proximity bias, and focus-window bias [10–18]. Geometrical biases are not under the scientist's control but can be dealt with on a theoretical basis. Measurement biases are related to the experimental setup: microscope magnification, use of reflected or transmitted light, oil immersion, inclusion of dipping tracks or TinCLEs and Cf or ion irradiation [4,19–24]. Measurement biases can be held in check by standardized procedures. Unintentional observer bias occurs when scientists measure different lengths on the same tracks. This effect is moderated by normalizing to a “zero” length specific to the scientist [7,8,25,26]. Intentional observer bias occurs when some confined tracks are selected for modeling and others are discarded as “not suitable for measurement”.

We proposed a track etch model for apatite and measured the corresponding etch rates [27–30]. This enables us, from the shape and size of a confined track, to infer its *c*-axis orientation, effective etch time and etch rate, in addition to its length. This releases us from the rigid etching protocols and provides insight into the relationship between etching and sampling biases. In this paper, we discuss how to optimize confined-track samples and the resulting thermal histories.

## 2. Step Etching

Figure 1 shows a horizontal confined induced track ( $\alpha\gamma$ ) at  $\sim 60^\circ$  to the *c*-axis in a prism face of Durango apatite after 15, 30 and 45 s immersion in 5.5 M HNO<sub>3</sub> at 21 °C [3]. It is intersected at  $\frac{1}{4}$  of its length by the host track ( $\beta$ ). It is widest at  $\beta$  and narrows towards  $\alpha$  and  $\gamma$ , implying a finite track etch rate  $v_T$  (symbols are explained in Supplement Table S1). The ruler-straight edges show that  $v_T$  is constant over almost its entire length [31]. The track width at  $\beta$  is  $\sim 0.9 \mu\text{m}$ , indicating that it was etched for the last  $\sim 7.4$  s of its immersion, while during the first  $\sim 7.6$  s the acid progressed down the host track and across to the confined track. For an average track etch rate  $v_T$  the tip ( $\alpha$ ) closest to  $\beta$  was etched for about five seconds, whereas ( $\gamma$ ) was etched for two seconds at most. Nevertheless,  $\gamma$  is rounded, which has been taken as a sign that the track is well-etched or even over-etched (Figure 7 in [10]). In contrast,  $\alpha$  just begins to develop a polygonal shape bounded by slow etching basal and prism faces (Figure 11 in [32]; Figure 2 in [27]), in agreement with the theories of crystal growth and dissolution (etching). In crystal growth and dissolution, rounded rather than polygonal forms require explaining (Figure 2a). However, that is straightforward: a constant  $v_T$  accounts for the straight track, a decreasing  $v_T$  accounts for the rounded tip (motorboat effect; Figure 1 in [31]) and zero  $v_T$  for the polygonal track tip determined by the apatite etch rates  $v_R$  (Figure 2b). Thus, it is not before a confined track has developed polygonal terminations at both ends that it can be considered fully etched.

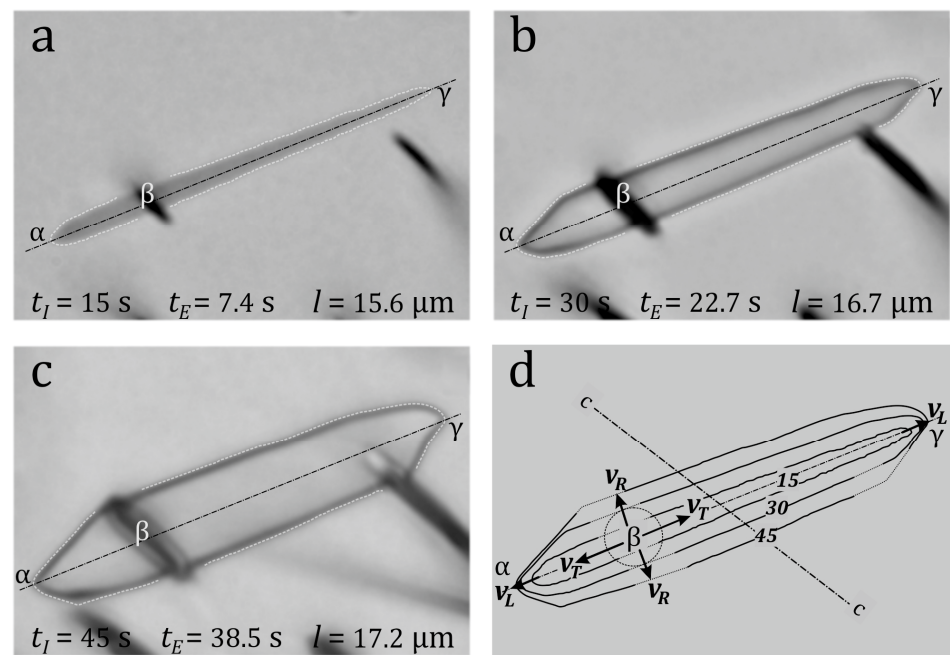


**Figure 1.** Unannealed horizontal induced confined track in Durango apatite after (a) 15 s, (b) 30 s and (c) 45 s of immersion in 5.5 M HNO<sub>3</sub> at 21 °C, and superimposed outlines (d);  $t_I$ : immersion time;  $t_E$ : effective etch time;  $l$ : track length  $c$ - $c$ : apatite  $c$ -axis;  $v_T$ : track etch rate;  $v_L$ : rate of length increase;  $v_R$ , apatite etch rate perpendicular to the track axis. The host track intersects at  $\frac{1}{4}$  track length from endpoint  $\alpha$ .

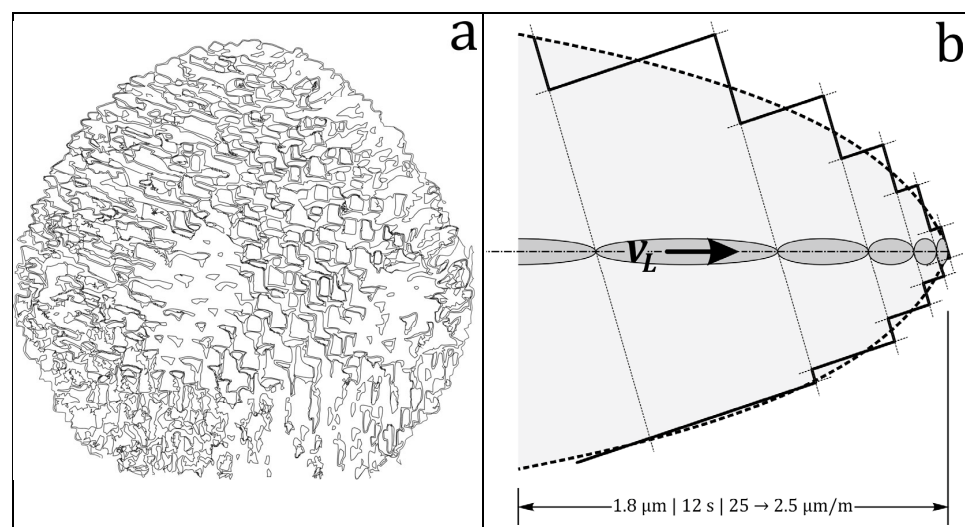


**Figure 2.** (a) Chemical etching of single-crystal spheres illustrates that rounded forms are not their natural boundaries (modified, after [33]). (b) The rounded track tip at  $\gamma$  in Figure 1 is the result of a decreasing track etch rate (motorboat effect; [31]) caused by an intermittent latent track structure [34].

After the second immersion, the width of the track in Figure 1 increases to three times that after the first immersion, and after the third to more than five times, whereas its length has increased <10%. This is because both ends become bounded by basal and prism faces, which limit the rate of length increase to that controlled by the lowest apatite etch rates. At high angles to the  $c$ -axis, the basal face grows faster in extent; at low angles, the prism face grows faster (Figure 11 in [32]; Figure 2 in [27]). A short etch produces thin tracks with rounded tips that are easier to measure but underetched, whereas a longer etch produces broad tracks with angular terminations that are overetched to an extent and appear more

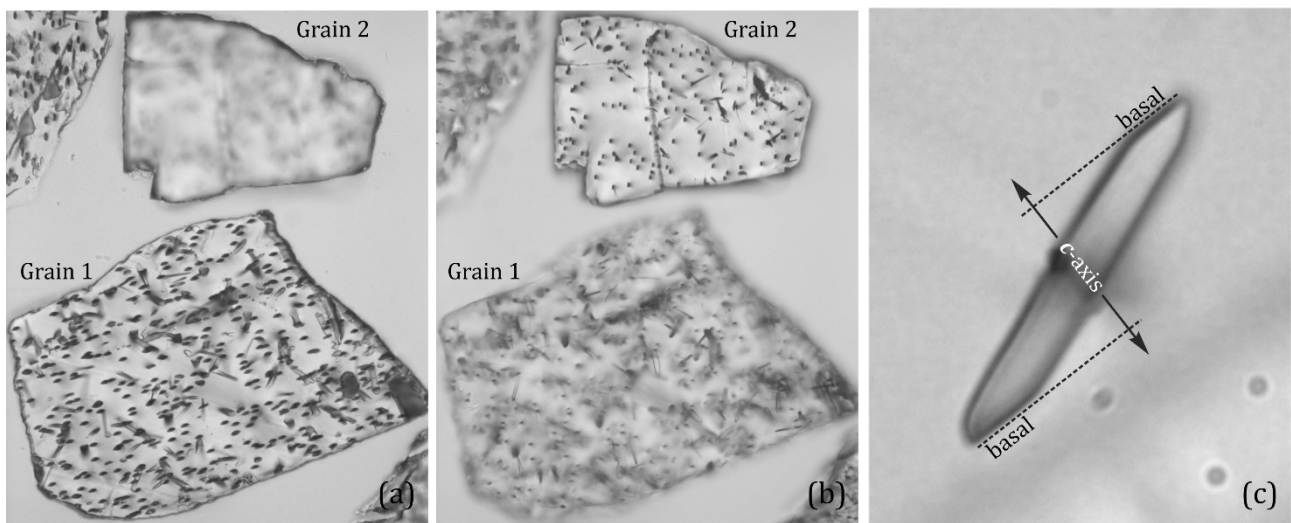
difficult to measure. However, per definition, it is right to measure the track length from the intersection between the basal and prism faces at one end of the track to that at its opposite end (Figure 1d). Supplement Figure S1 shows that the measurements of confined track lengths by two independent analysts are more consistent after 30 s of immersion (correlation coefficient  $r_l = 0.99$ ) than after 15 s ( $r_l = 0.95$ ); there is no further improvement after 45 s of immersion ( $r_l = 0.99$ ). The same appears to be the case for the track widths ( $w$ ) and effective etch times ( $t_E$ ). The fact that the etch times are less consistent than the widths underscores the importance of the track orientations ( $\phi$ ) for calculating the effective etch time  $t_E = \frac{1}{2} w/v_R(90 - \phi)$ .

Figure 1 illustrates that there is no time at which a confined track is well etched at both ends. At the moment that one end goes from track etching ( $v_T, v_L$ ) to bulk etching ( $v_R$ ), the other will be overetched if it is closer to the host track or underetched if it is more distant. Moreover, shorter tracks will, on average, be overetched relative to longer tracks [10]. Therefore, different confined tracks not only have different formation and geological histories but also different etching histories. The aim of etching protocols should be to minimize etching artifacts. This raises the question of what to aim for: an etching protocol that achieves the closest possible approximation to the intrinsic (latent) track lengths, or one that produces the best fit with the published annealing data on which the equations for modeling temperature–time paths (Tt modeling) are based. In either case, the next question is whether the goal is best achieved by a uniform standardized protocol or by protocols tailored to the etching properties of individual samples and tracks (fossil or induced).

### 3. Ion Irradiation

In addition to a representative sample and accurate measurements, the number of confined tracks is also important for modeling geological thermal histories. The common method to increase their number is to expose samples to fission fragments from a  $^{252}\text{Cf}$  source [35]. This creates semi-tracks that act as conduits along which the etchant gains access to fission tracks in the grain interior. “Cf-tracks” from “Cf-irradiation” intersect confined tracks within half a full track length below the surface. This method uses the same etch times as for unirradiated samples. The increase in the confined track sample can reach almost an order of magnitude in suitable apatite samples (Figure 3 in [35]) but appears to be less efficient for zircon [36]. These authors also studied artificial fracturing and accelerator-ion irradiation as alternatives to Cf irradiation, while [37] used extended etching to increase the sample size.

Ions from a linear accelerator can have GeV energies, allowing them to traverse entire apatite grains. However, confined tracks at  $\gtrsim 10\ \mu\text{m}$  depth are generally underetched at standard immersion times because of the time needed for the etchant to travel down the ion tracks. We are not bound by protocols if we can calculate the effective etch time of each confined track from its width at its intersection with the host track [27,29,30]. Then, it is advantageous to combine ion irradiation with an extended etch time or with step etching. The result depends on the sample, the beam properties and the etch protocol. Just increasing the immersion time, keeping all else constant, can increase the confined track sample size by an order of magnitude for the most part due to the widening of the ion tracks (Figures 3 and 6 in [38]). This approach has other advantages: Figure 3a,b show two apatite grains etched for 40 s in 5.5 M  $\text{HNO}_3$  at 21 °C. The focus difference between the fast-etching grain (grain 2) and the slow-etching grain (grain 1) facilitates rapid grain selection at moderate magnifications. Figure 3c shows a confined track well below the deepest surface tracks etched to a point where it is terminated at both ends by basal and prism faces. Thus, one well-etched confined track allows determination of the orientation of the apatite  $c$ -axis.



**Figure 3.** Two grains etched for 40 s in 5.5 M HNO<sub>3</sub> at 21 °C illustrate the contrast between fast- and slow-etching surfaces; the slow-etching prism surface (grain 1) is more or less still at the same level as that of the unetched mount, as indicated by its sharp outline in (a), whereas the surface of the fast-etching crystal (grain 2) has been lowered to a level so far below that of the mount that it is out of focus in (a); it comes into sharp focus after lowering the objective to the point where the image of grain 1 becomes blurred (b); (c) the outline of a single well-etched confined track allows one to determine the *c*-axis azimuth.

Ion irradiation reveals more non-horizontal confined tracks than Cf irradiation. Their lengths and orientations can be measured with dedicated software but also without. The ion tracks at a fixed angle ( $\delta$ ) to the surface allow converting a horizontal distance ( $p$ ) into a height ( $v$ ), requiring no correction for refraction. One measures the horizontal distances  $h$  and  $p$  and the apparent angle to the *c*-axis  $\alpha$  while focusing on the upper and lower ends of the confined track (Figure 4). Its true length  $l$  and *c*-axis angle  $\phi$  are then calculated as follows [39]:

$$l = \sqrt{h^2 + p^2 \tan^2 \delta}$$

$$\phi = \cos^{-1} \left( \frac{h}{l} \cos \alpha \right)$$

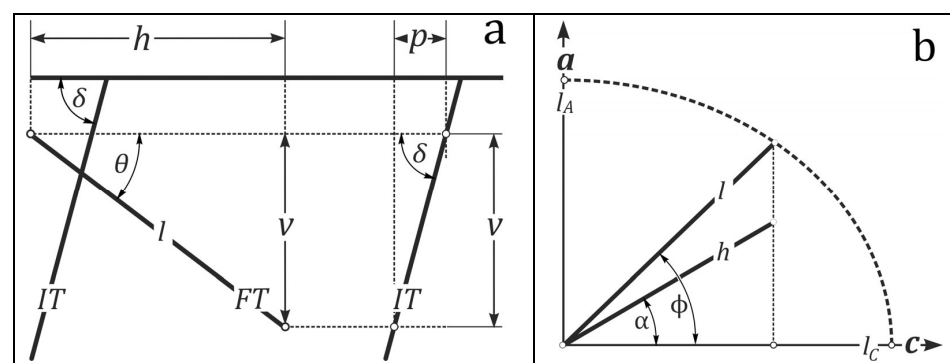


**Figure 4.** Calculation of (a) the length ( $l$ ) and (b) the *c*-axis angle ( $\phi$ ) of a dipping confined fission track (FT) from measurements of its projection ( $h$ ) and of a section of ion track (IT;  $p$ ) extending over the same depth ( $v$ ) as the fission track.

Measuring two or more ion tracks (averaging  $p$ ) around each confined track increases precision, which is at least as good as that of 3D length measurements on image stacks (Supplement Figure S2; [5]). In contrast to the orientation-dependent surface intersections of

fission tracks [40], the identical ion track openings also permit precise  $Dpar$  measurements. Video supplement S1 of an apatite grain irradiated with  $2.5 \times 10^6 \text{ cm}^{-2}$  Xe ions and etched for 40 s in 5.5 M  $\text{HNO}_3$  at 21 °C shows the potential of ion irradiation and an extended etch time.

#### 4. Apatite Etch Rates

As a result of their sub-microscopic diameters, fission tracks in apatite are made visible under an optical microscope by chemical etching. This is because the disordered region along the fission fragments' trajectories reacts faster with the etchant than the undisturbed lattice [41]. Fleischer and Price [42] described track development in polymers and glasses in terms of the etch rate  $v_T$  along the track and the bulk etch rate  $v_B$  of the track detector. With a notable exception [43], this concept was also adopted as a framework for describing track revelation in apatite [44,45], which affords the rationale for using slow-etching prism faces for dating. However, a  $(v_T, v_B)$  model cannot explain the varied appearances of etched fission tracks depending on their crystallographic orientation and that of the etched surface [32].

Aslanian et al. [27] proposed a model with three etch rates;  $v_T$  is as before the track etch rate, and  $v_R$  is the apatite etch rate. In contrast to  $v_B$ , which is the etch rate of a point on an etched surface (Huygens–Fresnel principle),  $v_R$  is the rate of displacement of a lattice plane, as in the theories of crystal growth and dissolution [46,47]. For practical reasons, we further define  $v_L$ , the rate of increase of confined track lengths;  $v_L$  is a combination of apatite ( $v_R$ ) and track etch rates ( $v_T$ ) that cannot be resolved into their components (Figure 2b).

Step-etch experiments are used for measuring etch rates [27,29,30,48];  $v_R$  is calculated from the increase in the width of confined tracks between consecutive immersions and  $v_L$  from their length increase (Figure 1);  $v_T$  is calculated from  $v_R$  and the angle between facing edges of the track channel [28]. Tracks with different orientations permit one to calculate  $v_R$ ,  $v_L$  and  $v_T$  as a function of the  $c$ -axis angle (Figure 5). The apatite etch rate  $v_R$  is lowest parallel and perpendicular to the  $c$ -axis and highest at  $\sim 20^\circ$  to  $c$ ;  $v_T$  differs from track to track, also with lower average values parallel and perpendicular to  $c$  [49]. Measurements of induced tracks in Durango apatite after 15, 30 and 45 s immersion in 5.5 M  $\text{HNO}_3$  at 21 °C yield decreasing  $v_T$  estimates because, during the second and third immersion, the etchant needs a finite time to reach the track tips again [30]. Thus, the first and highest estimates are closest to the true track etch rates  $v_T$ . Since the track length measures its extent of annealing,  $v_L$  has the greatest effect on the thermal histories of geological samples;  $v_L$  shows significant differences from track to track but on average no angular dependence; it can be higher or lower than the apatite etch rate along the axis of the track and decreases with increasing immersion time. This shows that  $v_L$  is a combination of track and apatite etch rates, which converges on continued etching to the lowest apatite etch rates as the influence of  $v_T$  decreases and vanishes when the tips become bounded by basal and prism faces (Figures 1, 2 and 5).

The etch rates allow us to calculate the duration for which individual confined tracks have been etched (effective etch time  $t_E$ ). This provides a quantitative criterion for judging whether a track is under- or overetched, and helps to assess the effect of the measured lengths on the thermal histories of geological samples. The practical advantage is that it frees us from adherence to protocols and allows adjusting the etching conditions to the properties of the samples.

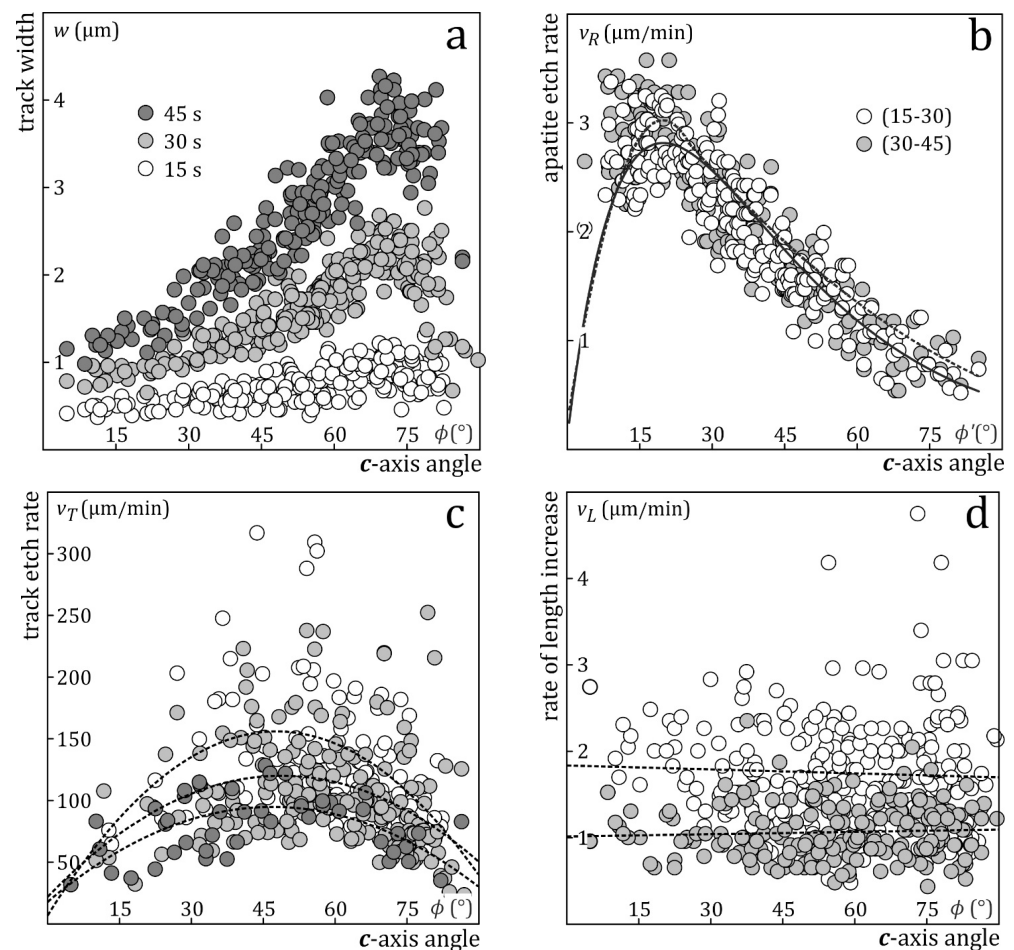


**Figure 5.** Track widths and etch rates vs. angle to the  $c$ -axis; (a) widths of induced confined tracks in Durango apatite after 15 s (no shading), 30 s (light shading) and 45 s (dark shading) of immersion in 5.5 M  $\text{HNO}_3$  at 21 °C vs. their  $c$ -axis angles ( $\phi$ ); (b) apatite etch rate  $v_R$  vs.  $c$ -axis angle of the etch rate vector ( $\phi' = 90 - \phi$ ), calculated from the width increase from 15 s to 30 s of immersion (no shading) and from 30 s to 45 s (light shading); dashed line: [27]; solid line: [29]; (c) track etch rate  $v_T$  vs. angle to the  $c$ -axis ( $\phi$ ); no shading: 15 s data; light shading: 30 s data, dark shading: 45 s data; the dashed lines are second-degree polynomial fits; (d) rate of length increase  $v_L$  vs. angle to the  $c$ -axis ( $\phi$ ), calculated from the length increase from 15 s to 30 s of immersion (no shading) and from 30 s to 45 s (light shading).

## 5. Immersion Time

Supplement Figure S3 shows a plot of the lengths of induced and fossil confined tracks in Durango apatite against effective etch time. It shows the striking difference between the low- $t_E$  interval, where different lengths increase at different rates, and the high- $t_E$  region, where most lengths increase at about the same rate. The different rates at low  $t_E$  reflect the etching histories of the tracks. At higher  $t_E$ , the tracks enter the bulk etching stage. From then on, their lengths increase at a constant rate in all directions (Figure 11 in [32]). Their etching histories are overwritten and the lengths of induced tracks come to reflect their formation histories, related to the masses, charges, energies and trajectories of the fission fragments. Their lengths continue to increase with  $t_E$  but the differences between them change little. The length differences between the fossil tracks come to reflect their combined formation and geological (thermal) histories. It is interesting to speculate if the order of their lengths continues to reflect their formation histories or if there are significant crossovers due to the different individual thermal histories of the tracks. This is more likely to be the case in cases of slow cooling than rapid cooling.

Figure 6a plots the measured lengths of induced tracks in Durango apatite against their effective etch times. The fitted power function shows that most tracks reach something close to their full lengths in a matter of seconds, as reported for strong etchants (5.0–5.5 M HNO<sub>3</sub>; [2–4,10,50]). This supports an average track etch rate  $v_T$  of the order of  $\sim 100 \mu\text{m}/\text{min}$  [18,27,29]. Their lengths thereafter increase at a diminishing rate. Figure 6b shows the track lengths normalized to their final values, measured after 45 s. This eliminates most of the intrinsic length differences between the tracks and reveals the general dependence of the confined track length on effective etch time. At  $t_E \lesssim 20$  s, the sample- $v_L$  is an average of tracks in less and more advanced etching stages. The offsets between them are due to their different lengths, etch rates  $v_T$  and intersection points with their host tracks. From  $t_E \gtrsim 20$  s onward, an increasing fraction enters the bulk etching stage, lowering the average  $v_L$ . At  $t_E \gtrsim 35$  s, all tracks are in bulk etching so that their lengths in all orientations increase at more or less the same rate (Figure 6 in [51]; Figure 11 in [32]; Figure 3 in [52]).

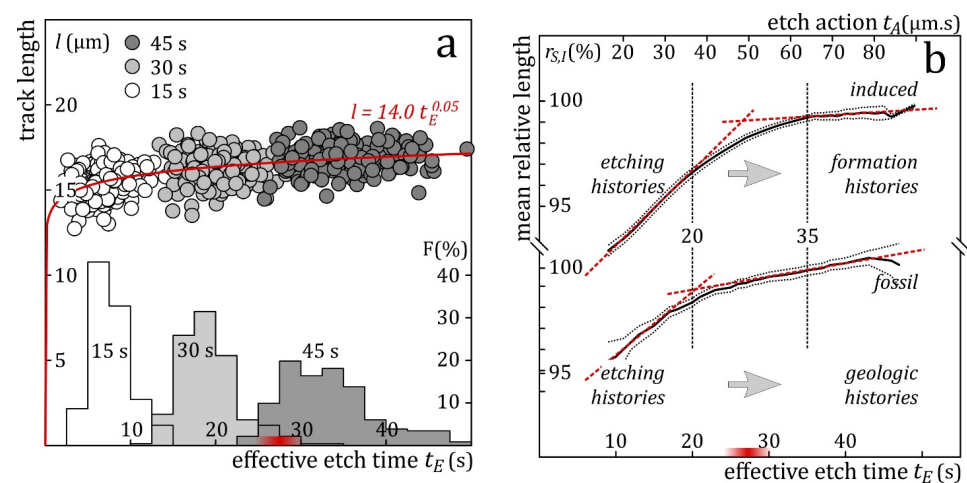


**Figure 6.** (a) Induced confined track lengths in Durango apatite plotted against the effective etch times calculated from their widths measured after 15 (white), 30 (light shading) and 45 s (dark shading) of immersion in 5.5 M HNO<sub>3</sub> at 21 °C; the histograms represent the effective etch time frequencies after 15, 30 and 45 s of immersion; (b) arithmetic means of the interpolated induced and fossil track lengths, normalized to their final values, plotted against effective etch time ( $t_E$ ; lower scale) and effective etch action ( $t_A = t_E \times D_{par}$ ; upper scale); solid line: mean normalized lengths; dotted lines:  $2\sigma$ -confidence interval of the mean. The dashed red lines have been added to illustrate linear sections; the red band at the bottom shows a suitable effective etch time interval for fossil and induced tracks in Durango apatite.

The fossil track data show the same general trend, except in certain details: (1) at  $t_E \lesssim 20$  s, the length increase of fossil tracks is slower than that of the induced tracks; (2) fossil tracks enter the bulk etching stage earlier than the induced tracks, and the transition is shorter and less gradual than that of the induced tracks; (3) from then on, their length increases faster than that of the induced tracks. The fossil track data are compiled from several experiments and are, thus, less homogeneous and perhaps less certain than the induced-track data. However, they are consistent with earlier reports that the track etch rate  $v_T$  of fossil tracks is generally lower than that of induced tracks [18,27,29], whereas the rate of length increase  $v_L$  due to bulk etching is higher [30,51]. The latter two observations are thought to be related to increased apatite etch rates due to the accumulated radiation damage in the samples with fossil tracks, which is annealed in the samples with induced tracks.

Plots of track length against effective etch time  $t_E$  are independent of the number of etch steps, of the immersion times and of the tracks selected for measurement. At  $t_E \gtrsim 35$  s, all induced tracks in Durango apatite are in “bulk etching”, of which a fraction is over-etched. Their mean length increases 2.5% from  $t_E = 20$  s to 35 s, 1.1% from 25 to 35 s and



0.4% from 30 to 35 s. Thus, it seems practical to aim for an average effective etch time of 25–30 s. Confined tracks in this interval have well-defined outlines (Figure 1b) and allow reproducible length and width measurements (Figure S1). In contrast to their lengths, the number of tracks in the chosen interval depends on the etch protocol and initial selection. Our three-step protocol is not efficient at generating confined tracks in the  $t_E$  range 25–30 s; after 15 + 15 s immersion, most tracks fall short of the goal, while after 15 + 15 + 15 s most tracks overshoot it (Figure 6a). A single 45 s immersion produces much the same tracks as after three 15 s steps but also a left tail, extending to a short  $t_E$ . A one-step immersion is thus more efficient at revealing an adequate number of confined tracks. A disadvantage of long immersion times, whether in a single step or several, is that the increasing dimensions of the etched surface tracks can obscure the confined tracks. On the other hand, an extended immersion time, combined with deep ion irradiation, allows measurement of confined tracks well below—and with minimal interference from—the surface tracks. In an ongoing investigation of geological fluorapatites, we combine deep ion irradiation with a single 40 s immersion in 5.5 M HNO<sub>3</sub> at 21 °C (Figure 3 and Video Supplement S1).

The definition of  $v_R$  requires that the apatite etch rate remains constant during the immersion time of a sample ( $t_I$ ; Figure 5a,b; [40]). It follows that  $v_R$  is interchangeable with  $t_I$  and that samples with equal  $v_R \times t_I$  are etched the same. This applies to the effective etch times  $t_E$  of confined tracks as well: those with the same  $v_R \times t_E$  have the same widths and shapes. This applies across apatite species. Their etch rates depend on their compositions and scale with  $Dpar$  [29,30,53,54]. Thus, it makes sense to plot step-etch data not against the etch or immersion time, but against etch action:  $t_A = Dpar \times t_E$  (or  $t_A = Dpar \times t_I$ ). Etch action can be understood as a theoretical etch (or immersion) time that produces identical tracks (or populations) in apatites with different etch rates. Figure 7a illustrates the power of  $t_A$ : it shows the mean interpolated lengths ( $l_M$ ) of step-etched fossil-confined tracks in five samples with different compositions, and  $Dpars$  ranging from 1.6  $\mu\text{m}$  to 4.6  $\mu\text{m}$  against  $t_A$ . From  $t_A \gtrsim 20 \mu\text{m}\cdot\text{s}$  onward, the rate of length increase in all five samples is the same. The constant rate also agrees with the fact that fossil tracks are in bulk etching at  $t_A \gtrsim 20 \mu\text{m}\cdot\text{s}$  (Figure 5b).

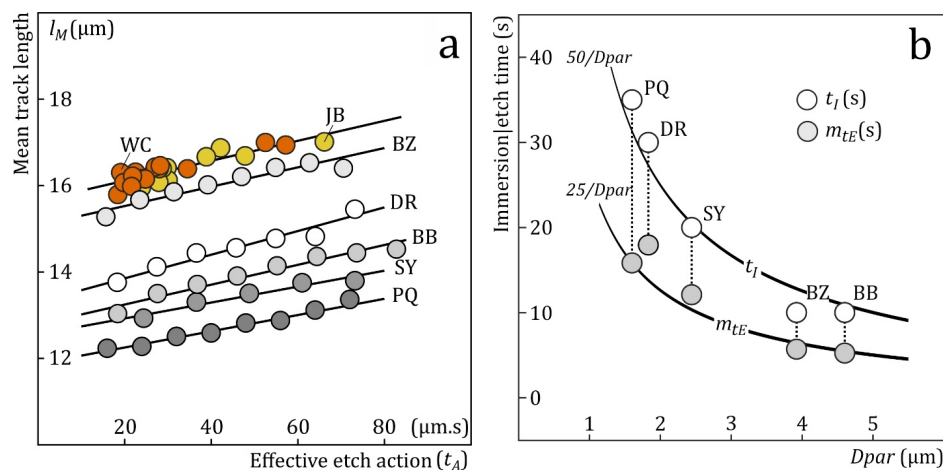


**Figure 7.** (a) Mean track length  $l_M$  vs. etch action  $t_A = Dpar \times t_E$ . Data: [27] (fossil tracks—DR, Durango), [29] (fossil tracks—BZ, Brazil, BB, Bamble, SY, Sludjanka, PQ, Panasqueira), [3] (induced tracks—WC) and [4] (induced tracks—JB). In the samples with fossil tracks, variation along the  $t_A$ -axis is due to step-etching and the associated increase in  $t_E$ , while  $Dpar$  is constant for each sample. In the case of the induced-track data, apatites with different compositions ( $Dpar$ ) were etched for the same immersion time  $t_I$ . For plotting the data, we assumed that their average effective etch times are half the immersion time:  $t_E \approx \frac{1}{2} t_I$ . (b) Aslanian et al. ([27]; DR) and Fu et al. ([29]; PQ, SY, BZ, BB) used immersion times  $t_I \approx 50 \times Dpar^{-1}$  for samples in the  $Dpar$  range 1.6–4.6  $\mu\text{m}$  etched in 5.5 M HNO<sub>3</sub> at 21 °C, resulting in mean effective etch times  $m(t_E) \approx 25 \times Dpar^{-1}$ .

Figure 7a also plots the mean lengths of induced tracks in other apatites, etched for the same immersion time, against  $t_A$  ([3]: 20 s in 5.5 M HNO<sub>3</sub> at 21 °C; [4]: 20 s in 5.0 M HNO<sub>3</sub> at 20 °C). In this case, the trend is due to different  $Dpar$ , not different  $t_E$ . The fact that the data define a common slope underscores that “etch action” has genuine meaning. It suggests that fission track etching is not so complicated that each factor must be considered on its own, and implies that confined track lengths can be corrected using a common rate of length increase. Therefore, it seems useful to recommend selecting immersion times for apatite in inverse proportion to  $Dpar$  ( $t_I = k \times Dpar^{-1}$ ; Figure 7b), which is the same as etching different samples to the same  $Dpar$ , as for zircon [55]. The value of  $k$  can be decided based on current estimates that the mean and standard deviation of the effective etch time distribution of the confined tracks are  $m(t_E) \approx \frac{1}{2} \times t_I$  and  $s(t_E) \approx \frac{1}{5} \times t_I$  for a single immersion step [29].

### 6. Length vs. Angle

Figure 8a plots the  $a$ - vs.  $c$ -axis intercepts of ellipses fitted to the length vs. orientation data for different confined-track samples [56]. The tracks in the unannealed and annealed induced-track samples ( $l_M$ : ~16 to ~10 μm) have “identical” thermal histories, and their  $a$ - and  $c$ -axis intercepts plot on a line:  $l_A = 1.632 l_C - 10.978$  [16,53]. Tracks in the fossil-track samples, on the other hand, have different geological thermal histories. Most fossil-track data plot above the induced-track line, i.e., fossil tracks appear to be more isotropic than induced tracks of comparable length. This is consistent with an earlier observation on 390 geological samples (Figure 12 in [53]), ascribed to suspected experimental factors related to the measurements and ellipse fitting. The scientists stressed the need for further investigation. Length bias complicates fitting ellipses to complex populations because the offsets between the constituent populations are greater at higher angles to the  $c$ -axis. Unequal angular distributions of the constituent populations with different degrees of annealing (Figure 5 in [16]) change the relative weights of the components at different  $c$ -axis angles. However, neither factor is expected to be of much consequence within the length range of our samples ( $l_C$  and  $l_A \gtrsim 10$  μm). For example, the simulated complex samples in Figure 8a deviate little from the induced-track line, even though several have standard deviations greater than 2.5 and even 3 μm.

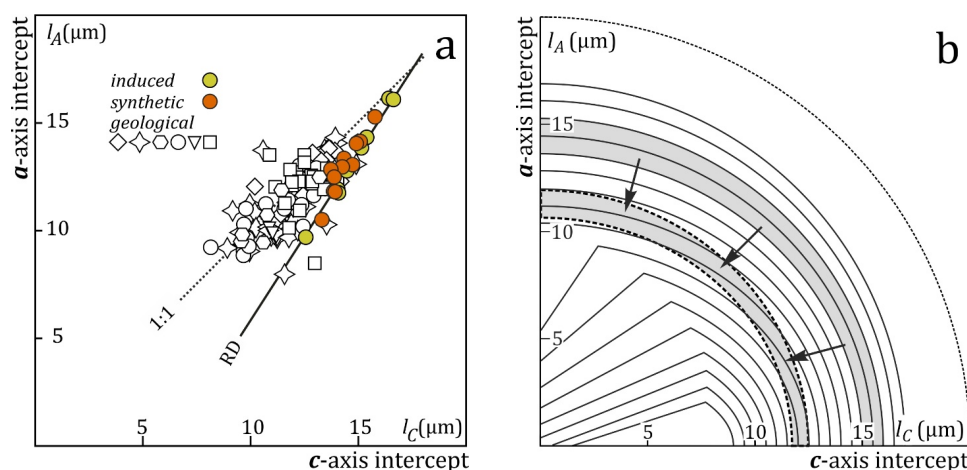


**Figure 8.** (a)  $a$ -axis vs.  $c$ -axis intercepts of ellipses fitted to (1) induced tracks annealed to different lengths (yellow), (2) simulated complex length distributions made by combining up to four induced-track samples into one (orange), (3) fossil-track samples from various geological studies (white). (b) Conceptual illustration of how underetching leads to more isotropic length distributions than expected for their means.

The offset of the fossil-track data from the induced-track model is, in our opinion, due to the fact that fossil tracks are underetched compared to induced tracks etched with the

same protocol. Figure 8b shows how an isotropic length deficit (arrows) results in more isotropic lengths than expected for a given mean. It also shows that the *c*-axis projection overestimates the *c*-axis equivalents of high-angle tracks relative to those of low-angle tracks. Apart from the ample data of [53] and in Figure 8a, etch experiments indicate that fossil tracks do not etch as induced tracks (Figure 6b), and there are indications from direct  $v_T$  measurements that the average etch rate of the fossil tracks in Durango apatite is lower than that of the induced tracks [18,27].

We interpolated the step-etch data (Supplement Figure S3) to obtain the track lengths at fixed effective etch times  $t_E$  and fitted ellipses to the length vs. orientation data ( $l$  vs.  $\phi$ ; Figure 9a) and straight lines to the *c*-axis-projected lengths vs. orientation data ( $l_P$  vs.  $\phi$ ; Figure 9b). At  $t_E = 10\text{--}15$  s, the track lengths are more isotropic than the model prediction, and the *c*-axis projection over-corrects the high-angle data, causing a regression line to  $l_P$  vs.  $\phi$  to have a positive slope. With increasing  $t_E$ , the track lengths increase in all directions (Figure 5d) until, at  $t_E = 20\text{--}30$  s, they are consistent with the model, and the regression line to  $l_P$  vs.  $\phi$  is horizontal (Figure 9b). With continued etching, the relationship is inverted as the track lengths become more anisotropic than the model predicts, and the regression line to  $l_P$  vs.  $\phi$  has a negative slope. T,t modeling of under- or overetched tracks produces artifactual thermal histories. A plot of *c*-axis-projected lengths vs. orientation is, therefore, a powerful tool for detecting such artifacts. It is reasonable to assume that track lengths consistent with this model are the best estimates of their true values, regardless of the etch protocol that produced them [30]. The best fit is obtained for effective etch times between 20 and 30 s, which correspond to longer immersion times than those of the annealing experiments on which the model is based [3,53]. As a result of differences between fossil and induced tracks (Figure 6b), and between scientists' selection criteria, it is not clear that strict adherence to the protocols underlying the annealing equations guarantees correct results, much like strict adherence to the  $\zeta$ -procedure does not ensure accurate ages [57,58].

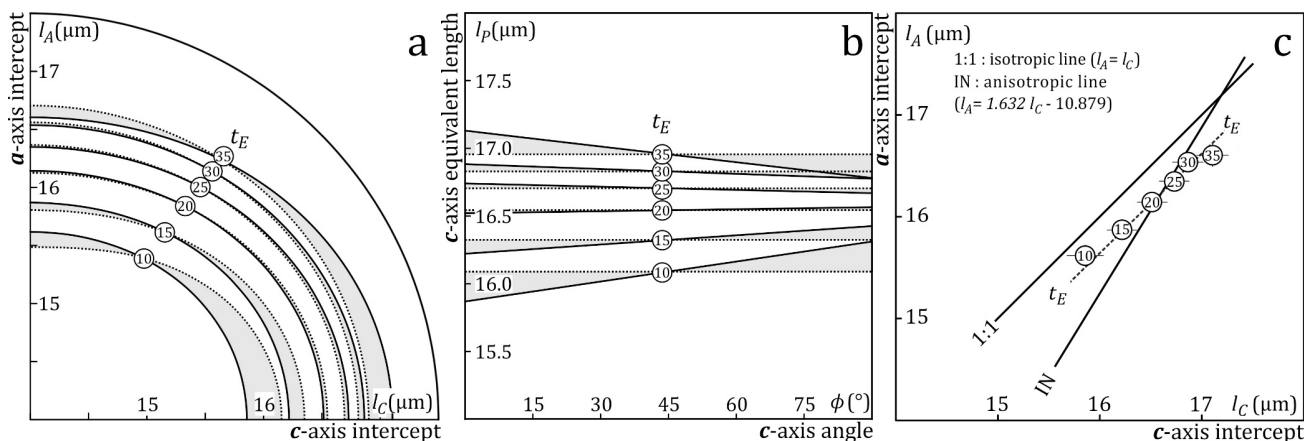


**Figure 9.** (a) Unconstrained (solid) and constrained (dotted lines;  $l_A = 1.632 l_C - 10.978$ ; [53]) ellipses fitted to the interpolated length and angle data for effective etch times of 10, 15, 20, 25, 30 and 35 s. (b) Unconstrained (solid) and constrained (dotted;  $l_A = l_C$ ) lines fitted to the *c*-axis projected lengths vs. *c*-axis angles. (c) The *a*-axis intercepts vs. *c*-axis intercepts of unconstrained ellipses fitted to the interpolated lengths and orientations of step-etched induced confined tracks in Durango apatite (Figure 9a).

Figure 9c plots the *a*-axis intercepts vs. *c*-axis intercepts of ellipses fitted to the orientations and interpolated lengths of induced tracks in Durango apatite at effective etch times  $t_E = 10\text{--}35$  s. At short  $t_E$ , the data plot above the model line for induced tracks, towards the isotropic line. With increasing  $t_E$ ,  $l_A$  and  $l_C$  increase at a diminishing rate (Figure 6) parallel to the isotropic line (Figure 5d) and at  $t_E = 20\text{--}30$  s cross the induced-track line [53,56].

Figure 10a plots step-etch data for fossil tracks in five apatite samples with different compositions and  $Dpar$  [29]. The data refer to immersion times rather than effective etch times, but that makes no difference for this discussion. After the first immersion for  $t_1 \approx 50/Dpar$  (Figure 7b), all samples, except Durango, plot above the model line for annealed induced tracks, towards the isotropic line. Of the five samples, PQ has the shortest mean confined track length ( $l_M = 12.3 \mu m$ ) with the greatest standard deviation ( $\sigma_M = 1.7 \mu m$ ). The values for all the samples are well outside the range for departures from the model line due to length bias or to unequal angular distributions of the constituents (Figure 5 in [16]; Figure 5 in [18]). Therefore, it is reasonable to conclude that the fossil tracks are underetched. Indeed, after an additional 15 s of immersion, four out of five samples agree with the expected trend.

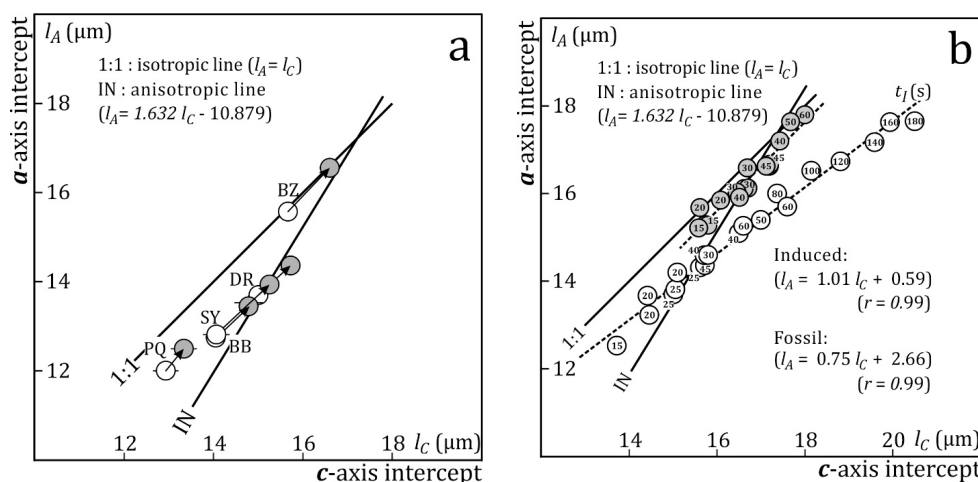


**Figure 10.** (a) The  $a$ -axis intercepts ( $l_A$ ) vs.  $c$ -axis intercepts ( $l_C$ ) of unconstrained ellipses fitted to the lengths and orientations of step-etched fossil confined tracks in apatites with different compositions (open circles: first step; filled circles: second step). Immersion times for the first step are shown in Figure 7b; the second measurement was performed after an additional immersion of 15 s in 5.5 M  $HNO_3$  at 21 °C [27,29]. (b) The  $a$ -axis intercepts vs.  $c$ -axis intercepts of unconstrained ellipses fitted to the lengths and orientations of step-etched fossil (filled) and induced (open) confined fission tracks in prism faces of Durango apatite etched for different immersion times ( $t_i$ ; numbers inside circles).

The increase in the fossil-track lengths after the second immersion appears at first to be isotropic, like the induced tracks. However more extensive step-etch data for fossil and induced tracks in Durango apatite indicate that there is a difference (Figure 10b). The increase in the induced track length is isotropic, but the lengths of low-angle fossil tracks appear to increase at a somewhat faster rate than those of high-angle tracks. This could be related to radiation damage or defects in the unannealed samples having a greater effect on the etch rate of basal faces than on that of prism faces. Despite the lack of empirical evidence, this is a reasonable assumption because basal faces are F-faces whose etch rate is more susceptible to defects than that of prism faces, which are S-faces ([59]; Figure 4 in [32]). It is not possible at this point to determine if this trend is the same for all fossil-track samples.

### 7. Conclusions

The related issues of etching protocol and track selection are difficult to untangle. There is currently no universal protocol for the different  $HNO_3$  concentrations in use in different laboratories. Based on our experiments with 5.5 M  $HNO_3$  at 21 °C [3], we propose that the immersion time should be matched to the apatite etch rate, e.g.,  $t_1 (s) \approx 50 (\mu m.s) / Dpar (\mu m)$ , assuming that  $Dpar$  is known. This is equivalent to etching different apatites to the same  $Dpar$ . The immersion time for Durango apatite is  $t_1 \approx 50/1.85 \approx 27$  s. This is just an estimate; in practice, we used  $t_1 = 30$  s, which produces a large number of confined tracks terminated by basal and prism faces at both ends, enabling consistent length measurements by experienced scientists

and permitting one to orient individual tracks relative to the  $c$ -axis. The  $D_{par}$  criterion implies that different immersion times are required for the components of multi-compositional samples. However, provided it is long enough, the immersion time is not so critical if the effective etch times ( $t_E$ ) of the selected tracks are calculated from their measured widths. Then, whether the sample is mono- or multi-compositional, it is possible to select the confined tracks suitable for modeling in accordance with each grain's  $D_{par}$ . Up to a point, the etchant concentration and immersion time are interchangeable in well-stirred solutions at constant temperature [51]. While it is not to be relied upon, it could provide a first estimate of the immersion time for weaker etchants than used in this research, until an empirical value is determined.

However, this does not, in general, guarantee that a confined track sample is suitable for modeling. The lengths of fossil tracks in geological samples are often more isotropic than expected for their average values, due to the fact that they are underetched compared to induced tracks. This should be assumed if a regression line fitted to  $l_P$  vs.  $\phi$  (Figure 9b) has a positive slope or the semi-axes ( $l_C, l_A$ ) of an ellipse fitted to  $l$  vs.  $\phi$  (Figure 9a) plot above the induced-track line (Figure 9c). In that case, an additional etch can increase the track lengths until they are consistent with the model based on annealing of induced tracks, a condition for valid thermal histories. It is not clear how long a second immersion should be, or even if model-consistent track lengths can be obtained within practical etch-time limits. However, if the widths of confined tracks are measured, along with their lengths and orientations, it should be possible to select a subset with effective etch times that are consistent with the model. If a second etch is not possible, e.g., because the mount was irradiated after the first etch, one might attempt to achieve the same result with numerical means, i.e., by increasing the measured lengths by a fixed amount until the regression line to  $l_P$  vs.  $\phi$  is flat or ( $l_C, l_A$ ) plot on the induced-track line. For modeling, this can come down to lowering the "zero-length" ( $l_0$ ), albeit to values below measured initial lengths or calculated from compositional data. These remedies are imperfect, but the alternative of modeling data that are not consistent with the model is doubtful to yield valid thermal histories.

There is a growing interest in integrating thermochron data on regional and larger scales. This can involve merging newer and older data from labs using different protocols. We suggest that, where the track lengths and angles are available,  $l_P$  vs.  $\phi$  and  $l_A$  vs.  $l_C$  plots can help to evaluate the thermal histories. If unirradiated mounts are available, an additional etch and re-measurement of the track widths as well as their lengths and angles could offer a solution. It would be interesting to see how this affects the late worldwide exhumation and the geological bias for curvilinear over lab-based linear annealing equations.

**Supplementary Materials:** The following supporting information can be downloaded at: <https://www.mdpi.com/article/10.3390/min14101016/s1>, Figure S1: Comparison of independent track-length (a–c) and effective-etch-time (d–f) measurements by two analysts. In both cases, the agreement is greater for samples etched for 30 s in 5.5 M HNO<sub>3</sub> at 21 °C than for those etched for 15 s, but does not improve thereafter. Figure S2: Measurement of dipping confined induced fission tracks in ion-irradiated prism faces of Durango apatite; dark shading: apparent length vs. apparent angle (Figure 4:  $h$  vs.  $\alpha$ ); light shading: true length vs. true  $c$ -axis angle ( $l$  vs.  $\phi$ ); white:  $c$ -axis equivalent length vs.  $c$ -axis angle ( $l_P$  vs.  $\phi$ ). (a) Unannealed; (b) annealed for 1 h at 300 °C; (c) annealed 1 h at 300 °C; (d) annealed 1 h at 300 °C. Figure S3: Lengths of horizontal confined tracks vs. effective etch time; the lines connect the measurements for each track after 15 s, 30 s and 45 s of immersion in 5.5 M HNO<sub>3</sub> at 21 °C; (a) induced tracks; (b) fossil tracks; individual tracks are shown in a different color. Video supplement: transmitted-light microscope recording of the prism face of an apatite from the *Kontinentale Tiefbohrung* (1129 m); the mount was irradiated with 11.1 MeV/amu Xe ions at 15° and etched for 40 s in 5.5 M HNO<sub>3</sub> at 21 °C, revealing numerous confined tracks throughout the grain. Table S1: List of symbols.

**Author Contributions:** Conceptualization, administration, funding acquisition, supervision, original draft: R.J.; methodology, validation, formal analysis, investigation, resources, data curation, writing, visualization: R.J., C.A., H.F. and F.T. All authors have read and agreed to the published version of the manuscript.

**Funding:** This research was funded by the German Research Council (Deutsche Forschungsgemeinschaft project Jo 358/4).

**Data Availability Statement:** Original data for this research are included in the Supplements; other data used are from cited publications.

**Acknowledgments:** We are indebted to F. Krieger and L. Sarkosh for contributions to the data, to C. Trautmann and E. Toimil-Molares for irradiations at the GSI Helmholtzzentrum für Schwerionenforschung in Darmstadt and to Jie Liu for irradiations at the HIRFL Heavy Ion Research Facility in Lanzhou, China. This research benefited much from the comments of P.K. Jensen and two anonymous reviewers.

**Conflicts of Interest:** The authors declare no conflict of interest.

## References

1. Gleadow, A.J.W.; Duddy, I.R.; Green, P.F.; Lovering, J.F. Confined Fission Track Lengths in Apatite: A Diagnostic Tool for Thermal History Analysis. *Contrib. Mineral. Petrol.* **1986**, *94*, 405–415. [[CrossRef](#)]
2. Green, P.F.; Duddy, I.R.; Gleadow, A.J.W.; Tingate, P.R.; Laslett, G.M. Thermal Annealing of Fission Tracks in Apatite 1. A Qualitative Description. *Chem. Geol.* **1986**, *59*, 237–253. [[CrossRef](#)]
3. Carlson, W.D.; Donelick, R.A.; Ketcham, R.A. Variability of Apatite Fission-Track Annealing Kinetics: I. Experimental Results. *Am. Mineral.* **1999**, *84*, 1213–1223. [[CrossRef](#)]
4. Barbarand, J.; Hurford, T.; Carter, A. Variation in Apatite Fission-Track Length Measurement: Implications for Thermal History Modelling. *Chem. Geol.* **2003**, *198*, 77–106. [[CrossRef](#)]
5. Tamer, M.T.; Chung, L.; Ketcham, R.A.; Gleadow, A.J.W. Analyst and Etching Protocol Effects on the Reproducibility of Apatite Confined Fission-Track Length Measurement, and Ambient-Temperature Annealing at Decadal Timescales. *Am. Mineral.* **2019**, *104*, 1421–1435. [[CrossRef](#)]
6. Miller, D.S.; Crowley, K.D.; Dokka, R.K.; Galbraith, R.F.; Kowallis, B.J.; Naeser, C.W. Results of Interlaboratory Comparison of Fission-Track Ages for the 1992 Fission Track Workshop. *Nucl. Tracks Radiat. Meas.* **1993**, *21*, 565–573. [[CrossRef](#)]
7. Ketcham, R.A.; van der Beek, P.; Barbarand, J.; Bernet, M.; Gautheron, C. Reproducibility of Thermal History Reconstruction From Apatite Fission-Track and (U-Th)/He Data. *Geochem. Geophys. Geosy.* **2018**, *19*, 2411–2436. [[CrossRef](#)]
8. Ketcham, R.A.; Carter, A.; Hurford, A.J. Inter-Laboratory Comparison of Fission Track Confined Length and Etch Figure Measurements in Apatite. *Am. Mineral.* **2015**, *100*, 1452–1468. [[CrossRef](#)]
9. Ketcham, R.A.; Donelick, R.A.; Balestrieri, M.L.; Zattin, M. Reproducibility of Apatite Fission-Track Length Data and Thermal History Reconstruction. *Earth. Planet. Sci. Lett.* **2009**, *284*, 504–515. [[CrossRef](#)]
10. Laslett, G.M.; Gleadow, A.J.W.; Duddy, I.R. The Relationship between Fission Track Length and Track Density in Apatite. *Nucl. Tracks* **1984**, *9*, 29–38. [[CrossRef](#)]
11. Laslett, G.M.; Kendall, W.S.; Gleadow, A.J.W.; Duddy, I.R. Bias in Measurement of Fission-Track Length Distributions. *Nucl. Tracks* **1982**, *6*, 79–85. [[CrossRef](#)]
12. Galbraith, R.F.; Laslett, G.M.; Green, P.F.; Duddy, I.R. Apatite Fission Track Analysis: Geological Thermal History Analysis Based on a Three-Dimensional Random Process of Linear Radiation Damage. *Philos. Trans. Roy. Soc. Lond. A* **1990**, *332*, 419–438.
13. Jensen, P.K.; Hansen, K.; Kunzendorf, H. A Numerical Model for the Thermal History of Rocks Based on Confined Horizontal Fission Tracks. *Nucl. Tracks Radiat. Meas.* **1992**, *20*, 349–359. [[CrossRef](#)]
14. Galbraith, R.F. Some Remarks on Fission-Track Observational Biases and Crystallographic Orientation Effects. *Am. Mineral.* **2002**, *87*, 991–995. [[CrossRef](#)]
15. Galbraith, R.F. *Statistics for Fission Track Analysis. Interdisciplinary Statistics Series*; Chapman and Hall/CRC, Taylor and Francis Group: Boca Raton, FL, USA, 2005; 219p.
16. Ketcham, R.A. Observations on the Relationship between Crystallographic Orientation and Biasing in Apatite Fission-Track Measurements. *Am. Mineral.* **2003**, *88*, 817–829. [[CrossRef](#)]
17. Ketcham, R.A. Forward and Inverse Modeling of Low-Temperature Thermochronometry Data. *Rev. Mineral. Geochem.* **2005**, *58*, 275–314. [[CrossRef](#)]
18. Jonckheere, R. On Etching, Selection and Measurement of Confined Fission Tracks in Apatite. *Geochron. Discuss.* **2023**; preprint. [[CrossRef](#)]
19. Watt, S.; Green, P.F.; Durrani, S.A. Studies of Annealing Anisotropy of Fission Tracks in Mineral Apatite Using Track-in-Track (Tint) Length Measurements. *Nucl. Tracks Radiat. Meas.* **1984**, *8*, 371–375. [[CrossRef](#)]
20. Watt, S.; Durrani, S.A. Thermal Stability of Fission Tracks in Apatite and Sphene: Using Confined Track Length Measurements. *Nucl. Tracks* **1985**, *10*, 349–357. [[CrossRef](#)]
21. Crowley, K.D.; Cameron, M.; Schaefer, L. Experimental Studies of Annealing of Etched Fission Tracks in Fluorapatite. *Geochim. Cosmochim. Acta* **1991**, *55*, 1449–1465. [[CrossRef](#)]
22. Ketcham, R.A.; Donelick, R.A.; Carlson, W.D. Variability of Apatite Fission-Track Annealing Kinetics: III. Extrapolation to Geological Time Scales. *Am. Mineral.* **1999**, *84*, 1235–1255. [[CrossRef](#)]

23. Li, Q.; Gleadow, A.; Seiler, C.; Kohn, B.; Vermeesch, P.; Carter, A.; Hurford, A. Observations on Three-Dimensional Measurement of Confined Fission Track Lengths in Apatite Using Digital Imagery. *Am. Mineral.* **2018**, *103*, 430–440. [[CrossRef](#)]
24. Tamer, M.T.; Ketcham, R.A. How Many vs. Which: On Confined Track Selection Criteria for Apatite Fission Track Analysis. *Chem. Geol.* **2023**, *634*, 121584. [[CrossRef](#)]
25. Kohn, B.P.; Gleadow, A.J.W.; Brown, R.W.; Gallagher, K.; O'Sullivan, P.B.; Foster, D.A. Shaping the Australian Crust over the Last 300 Million Years: Insights from Fission Track Thermotectonic Imaging and Denudation Studies of Key Terranes. *Aust. J. Earth Sci.* **2002**, *49*, 697–717. [[CrossRef](#)]
26. Spiegel, C.; Kohn, B.; Raza, A.; Rainer, T.; Gleadow, A. The Effect of Long-Term Low-Temperature Exposure on Apatite Fission Track Stability: A Natural Annealing Experiment in the Deep Ocean. *Geochim. Cosmochim. Ac.* **2007**, *71*, 4512–4537. [[CrossRef](#)]
27. Aslanian, C.; Jonckheere, R.; Wauschkuhn, B.; Ratschbacher, L. A Quantitative Description of Fission-Track Etching in Apatite. *Am. Mineral.* **2021**, *106*, 518–526. [[CrossRef](#)]
28. Jonckheere, R.; Aslanian, C.; Wauschkuhn, B.; Ratschbacher, L. Fission-Track Etching in Apatite: A Model and Some Implications. *Am. Mineral.* **2022**, *107*, 1190–1200. [[CrossRef](#)]
29. Fu, H.; Trilsch, F.; Jonckheere, R.; Ratschbacher, L. Compositional Effects on Etching of Fossil Confined Fission Tracks in Apatite. *Am. Mineral.* **2024**; *in press*. [[CrossRef](#)]
30. Trilsch, F.; Fu, H.; Jonckheere, R.; Ratschbacher, L. Effective Etch Times of Fossil Fission Tracks in Geological Apatite Samples and Impact on Temperature-Time Modeling. *Lithosphere* **2023**. [[CrossRef](#)]
31. Fleischer, R.L.; Price, P.B.; Woods, R.T. Nuclear-Particle-Track Identification in Inorganic Solids. *Phys. Rev.* **1969**, *188*, 563–568. [[CrossRef](#)]
32. Jonckheere, R.; Wauschkuhn, B.; Ratschbacher, L. On Growth and Form of Etched Fission Tracks in Apatite: A Kinetic Approach. *Am. Mineral.* **2019**, *104*, 569–579. [[CrossRef](#)]
33. Heimann, R.B. *Dissolution of Crystals. Theory and Practical Application. Applied Mineralogy*, 8th ed.; Springer: Vienna, Austria; New York, NY, USA, 1975; p. 270. (In German)
34. Paul, T.A.; Fitzgerald, P.G. Transmission Electron Microscopic Investigation of Fission Tracks in Fluorapatite. *Am. Mineral.* **1992**, *77*, 336–344.
35. Donelick, R.A.; Miller, D.S. Enhanced Tint Fission Track Densities in Low Spontaneous Track Density Apatites Using <sup>252</sup>Cf-Derived Fission Fragment Tracks: A Model and Experimental Observations. *Nucl. Tracks Radiat. Meas.* **1991**, *18*, 301–307. [[CrossRef](#)]
36. Yamada, R.; Yoshioka, T.; Watanabe, K.; Tagami, T.; Nakamura, H.; Hashimoto, T.; Nishimura, S. Comparison of Experimental Techniques to Increase the Number of Measurable Confined Fission Tracks in Zircon. *Chem. Geol.* **1998**, *149*, 99–107. [[CrossRef](#)]
37. Ito, H. On a Simple Approach to Increase TINT Numbers in Apatite. *Fiss. Track News Lett.* **2004**, *17*, 1–7. (In Japanese with English abstract).
38. Jonckheere, R.; Enkelmann, E.; Min, M.; Trautmann, C.; Ratschbacher, L. Confined Fission Tracks in Ion-Irradiated and Step-Etched Prismatic Sections of Durango Apatite. *Chem. Geol.* **2007**, *242*, 202–217. [[CrossRef](#)]
39. Jonckheere, R.; Ratschbacher, L. On Measurements of Non-horizontal Confined Fission Tracks. Abstracts of Thermo 2010. In Proceedings of the 12th International Conference on Thermochronology, Glasgow, UK, 16–20 August 2010; p. 120.
40. Sobel, E.R.; Seward, D. Influence of Etching Conditions on Apatite Fission-Track Etch Pit Diameter. *Chem. Geol.* **2010**, *271*, 59–69. [[CrossRef](#)]
41. Price, P.B.; Walker, R.M. Chemical Etching of Charged-Particle Tracks in Solids. *J. Appl. Phys.* **1962**, *33*, 3407–3412. [[CrossRef](#)]
42. Fleischer, R.L.; Price, P.B. Charged Particle Tracks in Glass. *J. Appl. Phys.* **1963**, *34*, 2903–2904. [[CrossRef](#)]
43. Maurette, M. Investigation of Heavy Ion Tracks in Natural Minerals of Terrestrial and Extra-Terrestrial Origin. *Bull. Soc. Franç. Minér. Crist.* **1966**, *89*, 41–75. (In French)
44. Tagami, T.; O'Sullivan, P.B. Fundamentals of Fission-Track Thermochronology. *Rev. Mineral. Geochem.* **2005**, *58*, 19–47. [[CrossRef](#)]
45. Hurford, A.J. An Historical Perspective on Fission-Track Thermochronology. In *Fission-Track Thermochronology and Its Application to Geology, Geography and Environment*; Malusà, M.G., Fitzgerald, P.G., Eds.; Springer: Cham, Switzerland, 2019; pp. 3–23.
46. Wulff, G. On the Question of the Growth and Dissolution Rate of Crystal Faces. *Z. Kristall.* **1901**, *34*, 449–530. (In German)
47. Gross, R. On the Theory of Growth and Dissolution Processes of Crystalline Matter. *Abh. Math. Phys. Leipzig* **1918**, *35*, 137–202. (In German)
48. Aslanian, C.; Jonckheere, R.; Wauschkuhn, B.; Ratschbacher, L. Short Communication: Experimental Factors Affecting Fission-Track Counts in Apatite. *Geochronology* **2022**, *4*, 109–119. [[CrossRef](#)]
49. Gleadow, A.J.W. Fission-Track Dating Methods: What Are the Real Alternatives? *Nucl. Tracks* **1981**, *5*, 3–14. [[CrossRef](#)]
50. Moreira, P.A.F.P.; Guedes, S.; Iunes, P.J.; Hadler, J.C. Fission Track Chemical Etching Kinetic Model. *Rad. Meas.* **2010**, *45*, 157–162. [[CrossRef](#)]
51. Jonckheere, R.; Tamer, M.T.; Wauschkuhn, B.; Wauschkuhn, F.; Ratschbacher, L. Single-Track Length Measurements of Step-Etched Fission Tracks in Durango Apatite: “Vorsprung Durch Technik”. *Am. Mineral.* **2017**, *102*, 987–996.
52. Tamer, M.T.; Ketcham, R.A. The Along-Track Etching Structure of Fission Tracks in Apatite: Observations and Implications. *Chem. Geol.* **2020**, *553*, 119809. [[CrossRef](#)]
53. Donelick, R.A.; Ketcham, R.A.; Carlson, W.D. Variability of Apatite Fission-Track Annealing Kinetics: II. Crystallographic Orientation Effects. *Am. Mineral.* **1999**, *84*, 1224–1234. [[CrossRef](#)]

54. Donelick, R.A.; O'Sullivan, P.B.; Ketcham, R.A. Apatite Fission-Track Analysis. *Rev. Mineral. Geochem.* **2005**, *58*, 49–94. [[CrossRef](#)]
55. Yamada, R.; Tagami, T.; Nishimura, S. Confined Fission-Track Length Measurement of Zircon: Assessment of Factors Affecting the Paleotemperature Estimate. *Chem. Geol.* **1995**, *119*, 293–306. [[CrossRef](#)]
56. Donelick, R.A. Crystallographic Orientation Dependence of Mean Etchable Fission Track Length in Apatite: An Empirical Model and Experimental Observations. *Am. Mineral.* **1991**, *76*, 83–91.
57. Gleadow, A.; Kohn, B.; Seiler, C. The Future of Fission-Track Thermochronology. In *Fission-Track Thermochronology and Its Application to Geology, Geography and Environment*; Malusa, M.G., Fitzgerald, P.G., Eds.; Springer: Cham, Switzerland, 2019; pp. 77–92.
58. Jonckheere, R.; Härtel, B.; Iwano, H. Fission-Track Age Calibration: Phi and Zeta, Never the Twain Shall Meet? *Chem. Geol.* **2024**, *648*, 121898. [[CrossRef](#)]
59. Hartman, P.; Perdok, W.G. On the Relations between Structure and Morphology of Crystals I. *Acta Crystallogr.* **1955**, *8*, 49–52. [[CrossRef](#)]

**Disclaimer/Publisher's Note:** The statements, opinions and data contained in all publications are solely those of the individual author(s) and contributor(s) and not of MDPI and/or the editor(s). MDPI and/or the editor(s) disclaim responsibility for any injury to people or property resulting from any ideas, methods, instructions or products referred to in the content.